
Article:
Vasconcelos, R.G.W., Walkley, B. orcid.org/0000-0003-1069-1362, Day, S. et al. (4 more authors) (2020) 18-month hydration of a low-pH cement for geological disposal of radioactive waste: The Cebama reference cement. Applied Geochemistry, 116. 104536. ISSN 0883-2927

https://doi.org/10.1016/j.apgeochem.2020.104536

18-month hydration of a low-pH cement for geological disposal of nuclear waste: The Cebama reference cement

Rita G. W. Vasconcelos[1], Brant Walkley[1,2], Sarah Day[3], Chiu C. Tang[3], Haris Paraskevoulakos[4], Laura J. Gardner[1] and Claire L. Corkhill[1*]

[1] NucleUS Immobilisation Science Laboratory, Department of Materials Science and Engineering, The University of Sheffield, UK

[2] Department of Chemical and Biological Engineering, The University of Sheffield, UK

[3] Diamond Light Source, Harwell Science and Innovation Campus, Didcot, UK

[4] School of Physics, The University of Bristol, Bristol, UK

* Corresponding author:

Tel: +44 (0) 1142223632

Email: c.corkhill@sheffield.ac.uk

Abstract

Low-pH cements are candidate materials for use in the construction of geological disposal facilities for the long-term management of nuclear waste. Since these facilities will operate over long time scales, the changes in mineralogy and microstructure require evaluation as a function of time. As a first step towards this understanding, the hydration of a standardised low-pH cement paste, known as the Cebama reference cement, was investigated over an 18-month period. Characterisation was performed at 28 days of curing, at 20°C and 40°C, and novel synchrotron radiation X-ray diffraction experiments were performed, *in-situ*, from 90 minutes to 18 months of curing. Concurrent solid state ^{29}Si and ^{27}Al MAS NMR data were acquired for parallel samples to quantify the extent of cement hydration and the composition and mean chain length of the predominant calcium aluminosilicate hydrate (C-(A)-S-H) reaction product. After 18 months, cement clinker phases were still present, highlighting the slow hydration kinetics of this low-pH cement. The data presented provide a benchmark for ongoing and future studies of low-pH cements in geological disposal environments, over extended time scales.

1. Introduction

Geological disposal, in a facility several hundreds of metres below the surface, has been selected as the most suitable solution for the long-term management of nuclear waste in a number of countries, including those in Europe, the USA and Japan. The Geological Disposal Facility (GDF) design is based on a multi-barrier concept, where natural and engineered barriers will be used together to contain and mitigate the release of radionuclides from the waste to the geo- and biospheres, allowing radioactive decay, over a period of 100,000 years, to occur without exposing the biosphere to radioactive elements.

Cementitious materials feature in all current international concepts for geological disposal of nuclear waste as, for example, waste encapsulation grouts, waste containers and backfills, seals and fracture grouts, tunnel/vault linings and supporting structures including floors, roadways, bulkheads and buttresses. Their use confers a number of advantages: low cost; simple to emplace; provision of radiation shielding; high surface area for sorption of radionuclides and; where used as a buffer material, provision of an alkaline environment, which decreases the solubility of cationic radionuclides.

Low-pH cement formulations are currently of interest for geological disposal of nuclear waste. It is envisaged that they will be used in GDF construction where a less alkaline environment (pH < 11) is required, for example, when in contact with the other natural or engineered barriers, especially those composed of clay (Calvo et al., 2010; Cau Dit Coumes et al., 2006; Codina et al., 2008). In the recent European project, Cement-based materials, properties, evolution and barrier functions (Cebama), a low-pH cement was developed by VTT (Technical Research Centre of Finland) as a baseline reference material for a range of studies on cement behaviour in geological disposal environments, with experiments performed by 27 consortium beneficiaries. The composition, based on the ternary mix design of Posiva (Finnish Nuclear Waste Management Organisation), has previously been studied for GDF deposition tunnel end plugs (Holt et al., 2014). It has a ternary binder composition of Portland cement (PC), silica fume and blast furnace slag (BFS). The addition of the latter two components to PC reduces the amount of portlandite ($Ca(OH)_2$) formed during the cement hydration reaction, and increases the amount of low Ca/Si ratio calcium silicate hydrate (C-S-H) formed, as a consequence of the pozzolanic reaction. This gives rise to a cement pore solution with lower pH than for PC with no supplementary cementitious material additions (Calvo et al., 2010; Cau Dit Coumes et al., 2006; Codina et al., 2008; Lothenbach et al., 2012).

The long-term behaviour of low pH cements is of importance to the developing safety case for the construction and post-closure of a geological disposal facility, in particular for understanding the cement mineralogy and microstructure (porosity) when in contact with clay buffers or with groundwater. Here we present the results of an ongoing 18-month investigation of the hydration of the Cebama reference cement paste. To elucidate the nature of the hydration reaction, a range of analytical techniques were employed after 28 days of curing, and novel *in-situ* synchrotron radiation X-ray Diffraction (SR-XRD) coupled with solid state magic angle spinning nuclear magnetic resonance (MAS NMR) spectroscopy were utilised to quantify the extent of cement hydration, C-(A)-S-H composition and mean chain length, from 90 minutes after mixing until 528 days (ca. 18 months) of curing.

2. Materials and Methods

2.1. Materials

Batches of Cebama reference cement paste were prepared using the formulation shown in Table 1, with a water/solid ratio (w/s) of 0.25. All materials were provided by VTT (Technical Research Centre of Finland). The cement paste was mixed by first adding silica fume, BFS and 15 wt.% of PC to the mixing bowl, slowly adding the water and superplasticiser, and hand mixing for 3 minutes. A high shear mixer was used until the paste became fluid and the remainder of the PC was added and shear mixed. The cement paste was placed in centrifuge tubes which were sealed and cured at 20 ºC and 40 ºC, at 95 % relative humidity for 526 days. Samples cured *in-situ* at Diamond Light Source were not temperature controlled, but experienced temperatures within the range of 20°C to 40°C. Immersion in acetone for 3 days was performed to stop the hydration of solid samples at specific time points.

Table 1. Cebama reference cement paste formulation (Vehmas et al., 2016).

Material	Content (kg m^{-3})
Portland cement (CEM I 42.5 MH/SR/LA)	1050
Silica fume	1100
BFS	650
Plasticizer pantarhit LK (FM)	12.6

The composition of each precursor material, as determined by X-ray Fluorescence (XRF, Panalytical Zetium), is given in Table 2.

Table 2. Major constituents of raw materials, as determined by XRF and represented as oxides (precision ± 0.1%).

(wt.%)	Portland Cement (PC)	Blast furnace slag (BFS)	Silica fume
Na_2O	0.1	0.6	0.3
MgO	0.9	8.2	0.8
Al_2O_3	3.8	10.1	0.4
SiO_2	21.9	34.8	95.5
P_2O_5	0.1	<0.05	<0.05
K_2O	0.6	0.6	1.0
CaO	65.5	39.8	0.8
TiO_2	0.2	1.9	<0.05
Mn_3O_4	0.3	0.4	<0.05
Fe_2O_3	4.8	1.0	0.8
BaO	0.05	0.06	<0.05
Loss Free Total	98.2	97.5	99.6

2.2. Analytical methods

2.2.1. Characterisation of precursor materials

Particle size distribution measurements of cement reagents listed in Table 1 were performed by laser granulometry using a Mastersizer 3000 PSA, and the results were analysed using Malvern Instruments software. The refractive indices used for Portland cement, silica fume and BFS were 1.3, 1.54 and 1.63, respectively. Phase identification of precursor materials was performed using X-ray Diffraction (XRD) data and Diffrac.EVA V4.1 software with the ICDD PDF4+ 2015 database. Samples were crushed to a powder and sieved to a size fraction of < 63 μm. A Bruker D2 Phaser diffractometer utilising a Cu Kα source (1.54 Å) and Ni filter was used and measurements were taken from 5° to 70° 2θ with a step size of 0.02° and 2 s counting time per step.

2.2.2. Ex-situ characterisation of cement hydration

Isothermal calorimetry was conducted on cement paste samples using a TA Instruments TAM Air calorimeter, at both 20°C and 40°C. For samples that were analysed at 40°C, prior to mixing, the raw materials and water were kept at this temperature. The materials were then mixed externally and 20 g of sample was placed in a plastic ampoule and then into the calorimeter for 7 days. Hardened cement pastes were analysed using a PerkinElmer Pyris 1 Thermogravimetric Analyser (TGA). Approximately 40 mg of cement powder was used. The temperature ranged from room temperature to 1000°C with a heating rate of 10°C m^{-1} under N_2 (nitrogen) atmosphere. A Hiden

Analytical mass spectrometer (HPR-20 GIC EGA) was used to simultaneously record the mass spectrometer signals for H_2O and CO_2 of the thermal degradation products.

Back scattered electron images were recorded using a Hitachi TM3030 Scanning Electron Microscope (SEM) operating with an accelerating voltage of 15 kV. Energy Dispersive X-ray (EDX) analysis was performed using a Quantax 70 software and elemental maps were collected for between 15 to 20 minutes across a representative sample area of approximately 250 µm × 250 µm.

Solid state single pulse ^{29}Si and ^{27}Al MAS NMR spectra were acquired on a Bruker Avance III HD 500 spectrometer at 11.7 T (B_0) using a 4.0 mm dual resonance CP/MAS probe, yielding a Larmor frequency of 99.35 MHz for ^{29}Si and 130.32 MHz for ^{27}Al. ^{29}Si MAS NMR spectra were acquired using a 4 µs non-selective (π/2) excitation pulse, a measured 15 s relaxation delay, a total of 512 scans and spinning at 12.5 kHz. ^{27}Al MAS NMR spectra were acquired using a 1.7 µs non-selective (π/2) excitation pulse, a measured 5 s relaxation delay, a total of 512 scans and spinning at 12.5 kHz. All ^{29}Si and ^{27}Al spectra were referenced to pure tetramethylsilane (TMS) and 1.0 M aqueous $Al(NO_3)_3$, respectively, at 0 ppm.

Deconvolutions of the ^{29}Si MAS NMR were performed using non-linear minimisation of the sum of squared errors using Gaussian curves (Massiot et al., 2002; Bernal et al., 2013; Myers et al., 2015). The minimum number of peaks possible were fitted. $Q^n(m\text{Al})$ classification were used in the analysis, where a Si tetrahedron is connected to *n*Si tetrahedra ($0 > n > 4$), and *m* is the number of neighbouring AlO_4 tetrahedra (Lothenbach et al., 2014). Calcium/silicon (Ca/Si) ratio, aluminium/silicon (Al/Si) ratio and the mean chain length (MCL) were calculated using Equations 1 – 3, from Richardson (2014):

$$\frac{Ca}{Si} = \frac{\frac{3}{2}Q^1 + \frac{2}{3}Q^2}{Q^1 + Q^2} \quad \text{(Eqn. 1)}$$

$$\frac{Al}{Si} = \frac{\frac{1}{2}Q^2(1Al)}{Q^1 + Q^2 + Q^2(1Al) + Q^3 + Q^3(1Al)} \quad \text{(Eqn. 2)}$$

$$MCL = \frac{2}{\left(\frac{Q^1}{Q^1 + Q^2 + Q^2(1Al) + Q^3 + Q^3(1Al)}\right)} \quad \text{(Eqn. 3)}$$

Small pieces of cured cement paste were placed into the sample holder of an Autopore V 9600 (Micromeritics Instruments) Mercury Intrusion Porosimeter (MIP) for analysis of porosity. The maximum pressure applied was 208 MPa, the surface tension was 485 mN/m and the contact angle was 130°. The smallest pore entry size detected by the equipment is approximately 0.003 µm. Additionally, porosity was measured by X-ray Computed Tomography (XCT) at The

University of Bristol, using a Zeiss Xradia 520 Versa S-ray microscope. The rotation stage position was set so the X-ray source-to sample distance was minimal and allowed a minimum voxel size of 1.5 micrometres. The exposure time for each projection was 2.0 seconds, leading to a scan-time of ~2 hours. Threshold segmentation of obtained data was performed using Avizo software, through the identification of different intensity values; the lower intensity regions were identified as voids and used as the threshold value to distinguish the pores/voids from the matrix of the sample. Porosity values were then obtained.

2.2.3. In-situ characterisation of cement hydration

In-situ characterisation of cement paste, during curing, was performed at Diamond Light Source (proposal no. EE10038), at Beamline I11 LDE. Technical descriptions of the beamline, the only facility in the world that allows monitoring of slow kinetic processes by Synchrotron Radiation X-ray Diffraction (SR-XRD), are given by Murray et al., (2017) with additional information on the I11 diffraction methodology by Thompson et al., (2009, 2011). The Cebama cement paste was prepared as described above and transferred into a kapton capillary with the aid of a vibrational device. Then, the filled kapton capillary was placed inside an 0.7 mm diameter quartz capillary, which was sealed at the end with superglue (to mitigate carbonation of the cement) and transferred immediately into the experimental hutch. The first scan was taken 90 minutes after mixing. A monochromatic beam, with a spot size of 400 μm^2, an energy of 25 keV and a variable wavelength of 0.41 - 0.62 Å was used for the experiment. Diffraction patterns were recorded using a pixel area detector, with an angular range between 2° and 36° 2θ with a varying step size, always of ≤ 0.05°. The detector measured diffraction patterns of the sample, and an external CeO_2 standard, after the following time points: (i) 90 minutes after mixing, (ii) then every 7 days for up to 90 days; (iii) then every month up to one year and; (iv) the final scan was taken at 17.3 months (527 days).

3. Results and Discussion

3.1. Precursor material characterisation

Particle size analysis of the precursor powders (Figure 1) shows that for PC and BFS, 50% of the particles were < 14 ± 1 μm and < 11 ± 1 μm, respectively. The wider particle size distribution presented by silica fume shows the agglomerative nature of this material; even with ultrasonic treatment of the powder, 50 % of the particles were < 18 ± 2 μm and 90 % were < 52 ± 2 μm,

showing that agglomeration had not been completely avoided (since the actual particle size of silica fume is smaller than that of PC).

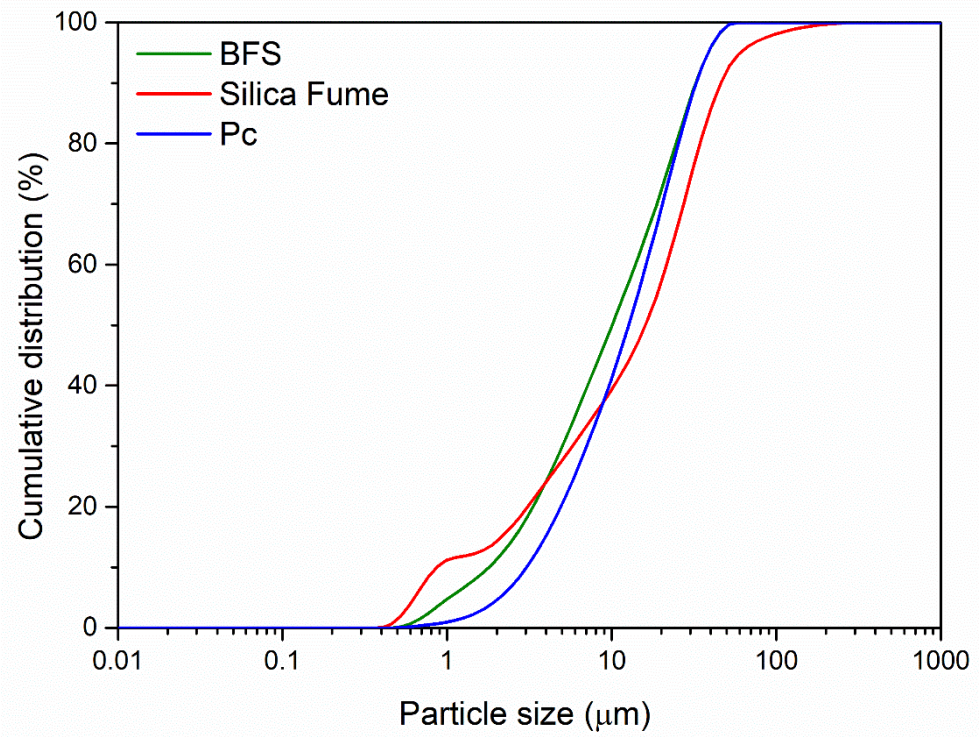

Figure 1. Particle size distribution of Portland cement (PC), blast furnace slag (BFS) and silica fume.

Through X-ray Diffraction analysis (Figure 2), it was possible to identify the mineralogy of the Cebama cement precursor materials. The PC CEM I 42.5N diffraction pattern (Fig. 2a) shows the expected clinker composition including: alite (Ca_3SiO_5; PDF 01-070-1846), belite (Ca_2SiO_4; PDF 01-086-0398 or 01-086-0399), aluminate ($Ca_3Al_2O_6$; PDF 01-070-0839), ferrite (Ca_2AlFeO_5; PDF 01-071-0667), gypsum ($CaSO_4{\cdot}2H_2O$; PDF 33-0311) and calcite ($CaCO_3$; PDF 01-086-0174). The presence of significant diffuse scattering features in the BFS and silica fume diffraction patterns (Figs. 2b and c) indicates the amorphous nature of these cementitious materials. It should be noted that the BFS also contains a small amount of calcite, and the silica fume contains a small amount of quartz.

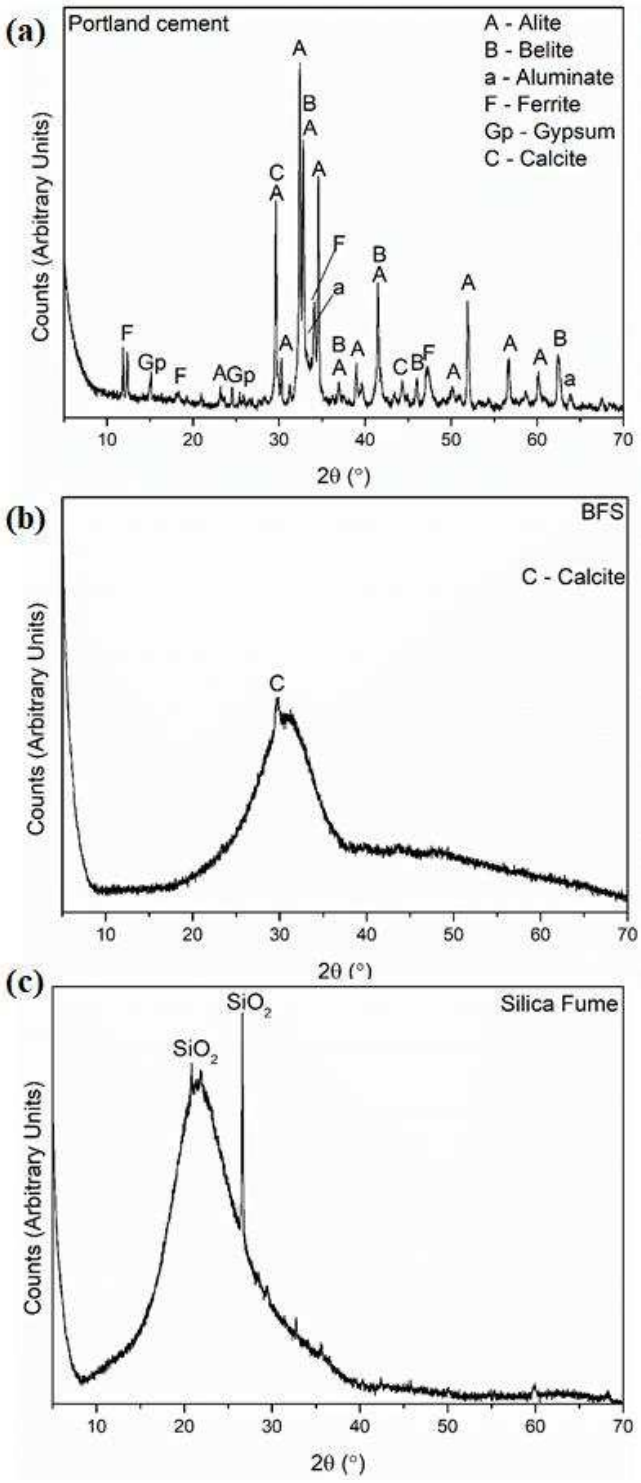

252

253 *Figure 2. X-ray diffraction patterns of: (a) PC; (b) BFS and; (c) silica fume.*

254

255

256

257

3.2. *Characterisation at 28 days of curing*

After 28 days of curing, the phase assemblage of the Cebama reference cement paste was determined by XRD, TG-MS and SEM techniques, the microstructure by porosity analysis, and the nanostructure by NMR spectroscopy.

XRD analysis revealed that the same phase assemblage was identified for materials cured at 20°C, 40°C and at Diamond Light Source in the I11 LDE hutch. Figure 3 highlights the phases identified, which include: calcite ($CaCO_3$; PDF 01-086-0174) (which overlaps with structurally disordered C-(A)-S-H; PDF 19-0052)); ettringite ($Ca_6Al_2(OH)_{12}(SO_4)_3{\cdot}26H_2O$; PDF 00-041-1451), hydrotalcite ($Mg_4Al_2(OH)_{14}{\cdot}3H_2O$; PDF 00-014-0191) and the AFm phase, monocarboaluminate ($Ca_4Al_2(OH)_{12}(CO_3)_3{\cdot}5H_2O$; PDF 01-087-0493). Some unreacted PC was observable as peaks of alite and belite. The diffuse scattering observed between 15 and 35° two theta indicate that unreacted BFS and silica fume were also present, in addition to C-S-H. The presence of low quantities of portlandite may be indicative of the limited reactivity of silica fume at early curing times; this may be a kinetic limitation (the pH is not high enough for the silica fume to react quickly) or related to mass transport – portlandite may not have been fully consumed by the pozzolanic reaction at this time. Previous studies observed the same hydrate phase composition for similar cement blends (Codina et al., 2008; Calvo et al., 2010).

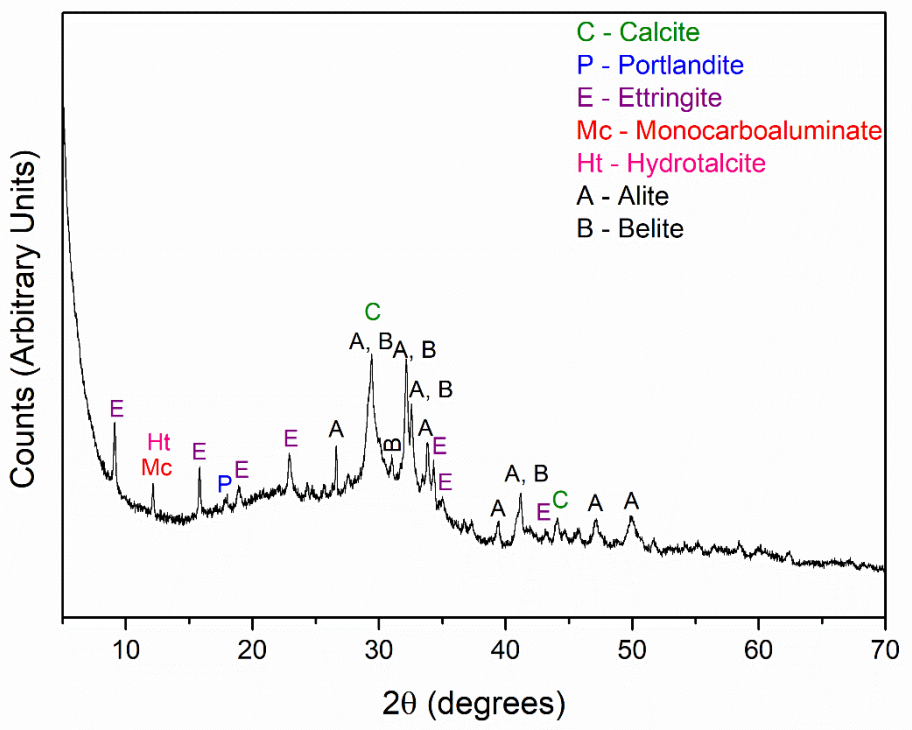

Figure 3. X-ray diffraction pattern of Cebama reference cement paste after 28 days of curing at 20 °C. NB: Additional AFm phases were identified by high resolution SR-XRD (see Figure 9).

The same phases as identified by XRD were apparent upon TG-MS analysis of samples cured at 20°C and 40°C for 28 days, shown in Figure 4. A broad peak corresponding to ettringite and AFm phases was observed between 100°C and 200°C (Scrivener et al., 2016), C-S-H was identified from the mass loss feature between 50°C and 100°C and, in agreement with its low quantity observed in the XRD pattern (Fig. 4), mass loss peaks relating to portlandite were not observed. At 40°C, the only difference was a slight increase in the width of the mass loss feature before 100°C – this may indicate that more C-S-H is formed in the cement cured at 40°C than 20°C, which is in good agreement with the isothermal calorimetry results (see below).

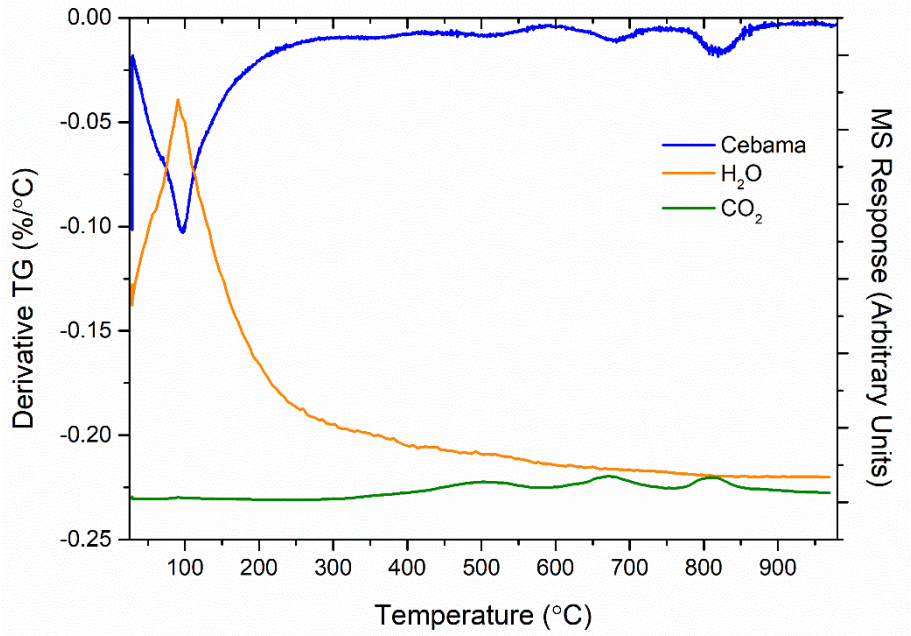

Figure 4. TGA-MS data for Cebama reference cement paste after 28 days of curing at 20°C.

In accordance with the particle size analysis results, which showed the agglomeration of silica fume particles, SEM imaging and EDX analyses (Figure 5) performed on samples cured at 20°C for 28 days showed that high speed shear mixing was not capable of completely disaggregating particles of silica fume (see particles labelled "A"). Also evident in SEM/EDX images were particles of BFS (labelled "B", Fig. 5); these are known to react slowly, especially in low-pH cement matrices (Richardson and Li, 2018). In terms of hydrate phases, C-S-H gel was identified as the matrix area (labelled "C", Fig. 5), surrounding particles of silica fume and BFS. The same phases and microstructure were observed for materials cured at 40°C.

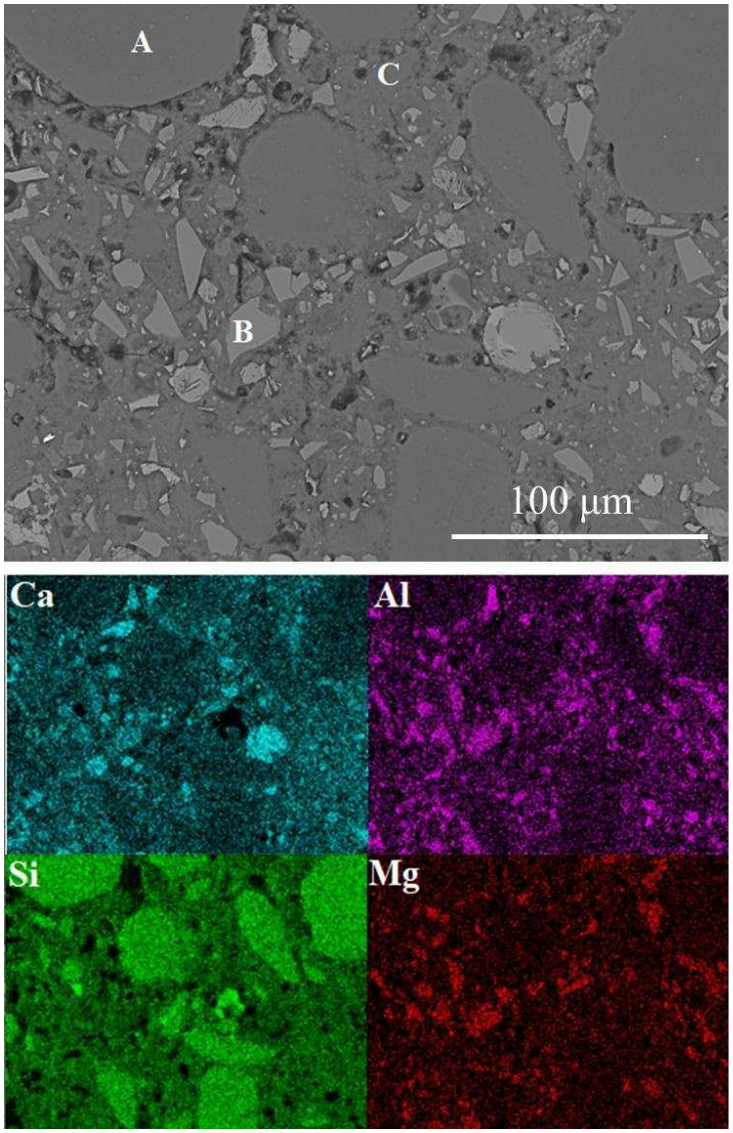

Figure 5. BSE SEM micrograph of Cebama reference cement paste after 28 days of curing at 20 °C, with the corresponding EDX maps for Ca, Al, Si and Mg.

The porosity of 28-day cured materials at 20°C and 40°C was determined using MIP (microporosity) and XCT (macroporosity) methods. Measurement by MIP (Figure 6) showed that, when cured at 20°C, the bulk of pores had entry sizes < 0.02 µm and the total porosity was around 16 ± 3 %. At 40 °C, the pore entry size diameter was mostly < 0.01 µm, and the total porosity was ~ 19 ± 3%. Essentially these values are the same, within error. When measured by XCT, the macroporosity of materials cured at both temperatures was ~3 ± 1 %.

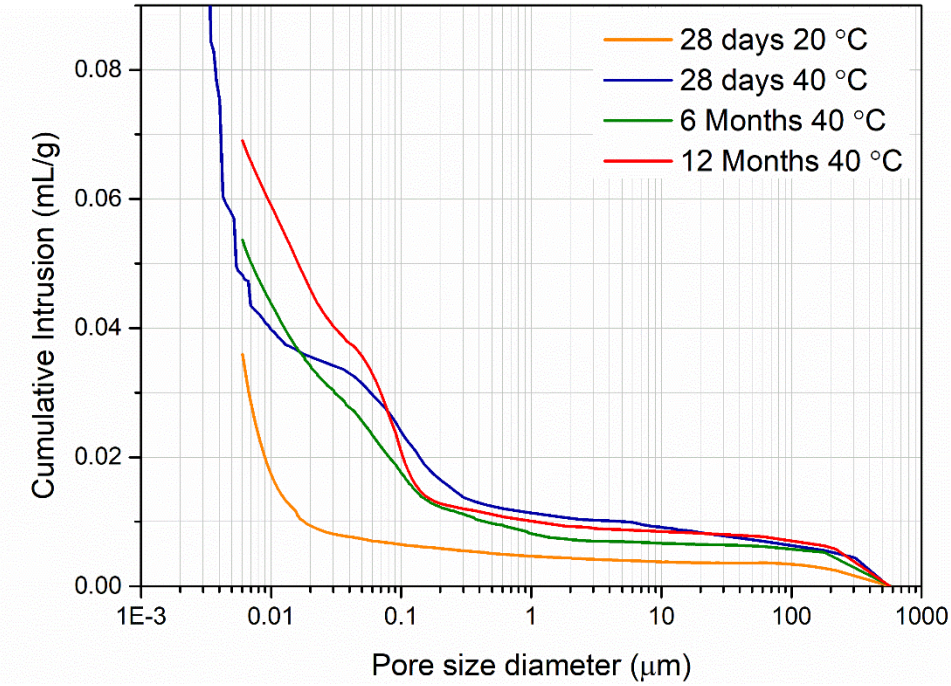

Figure 6. Pore entry size distribution of Cebama reference cement paste at different curing times and temperatures, determined using MIP.

^{29}Si MAS NMR and ^{27}Al MAS NMR was performed at 28 days of curing, as shown in Figure 7. In the ^{29}Si MAS NMR data, the presence of alite (isotropic chemical shift, δ_{iso} = -69 and -73 ppm) and belite (δ_{iso} = -70.8 ppm) (Scrivener et al., 2016) confirmed the presence of unreacted Portland cement after 28 days of curing (Fig. 7a). Two Q^1 environments (Q^1(I) at δ_{iso} = -73.9ppm and Q^1(II) at δ_{iso} = -78.9 ppm) were identified (Bernal et al., 2013; Myers et al., 2014; Prentice et al., 2018) and resonances exhibiting isotropic chemical shifts corresponding to the presence of Q^2(1Al) (δ_{iso} = -81.6 ppm), Q^2 (δ_{iso} = -84.5 ppm), Q^3 (δ_{iso} = -96.1 ppm) and Q^3(1Al) (δ_{iso} = -89.8 ppm) Si environments in C-A-S-H were also observed (Richardson, 2008; Richardson et al., 2004, 2010). A broad resonance resulting from remnant unreacted BFS was fitted underneath the Si environments in the reaction product (Prentice et al., 2018). The existence of Al within the first coordination sphere of Q^n Si sites demonstrates the incorporation of this element in an Al-substituted calcium silicate hydrate (C-A-S-H) binder phase. This was also visible in the ^{27}Al MAS NMR spectrum (Fig. 7b), from the presence of a broad tetrahedral Al peak (between δ_{obs} = 80 and 50 ppm) that contained contributions from Al^{IV} in C-A-S-H, and also from unreacted BFS (Andersen et al., 2003). In the octahedral Al region of Fig. 7b, a peak corresponding to ettringite (δ_{obs} = 14 ppm) and a small shoulder at the chemical shift of around δ_{obs} = 9 ppm, corresponding to the presence of AFm and hydrotalcite-like phases, was also identified (Andersen et al., 2003; Walkley and Provis, 2019). These results are in agreement with the XRD (Fig. 3) and TG-MS (Fig. 4) data. At 40°C, the same phases were identified, however, the intensity of the peak

corresponding to ettringite was greater than at 20°C (data not shown) due to the slightly higher rate of hydration observed at this temperature as determined by isothermal calorimetry (see below).

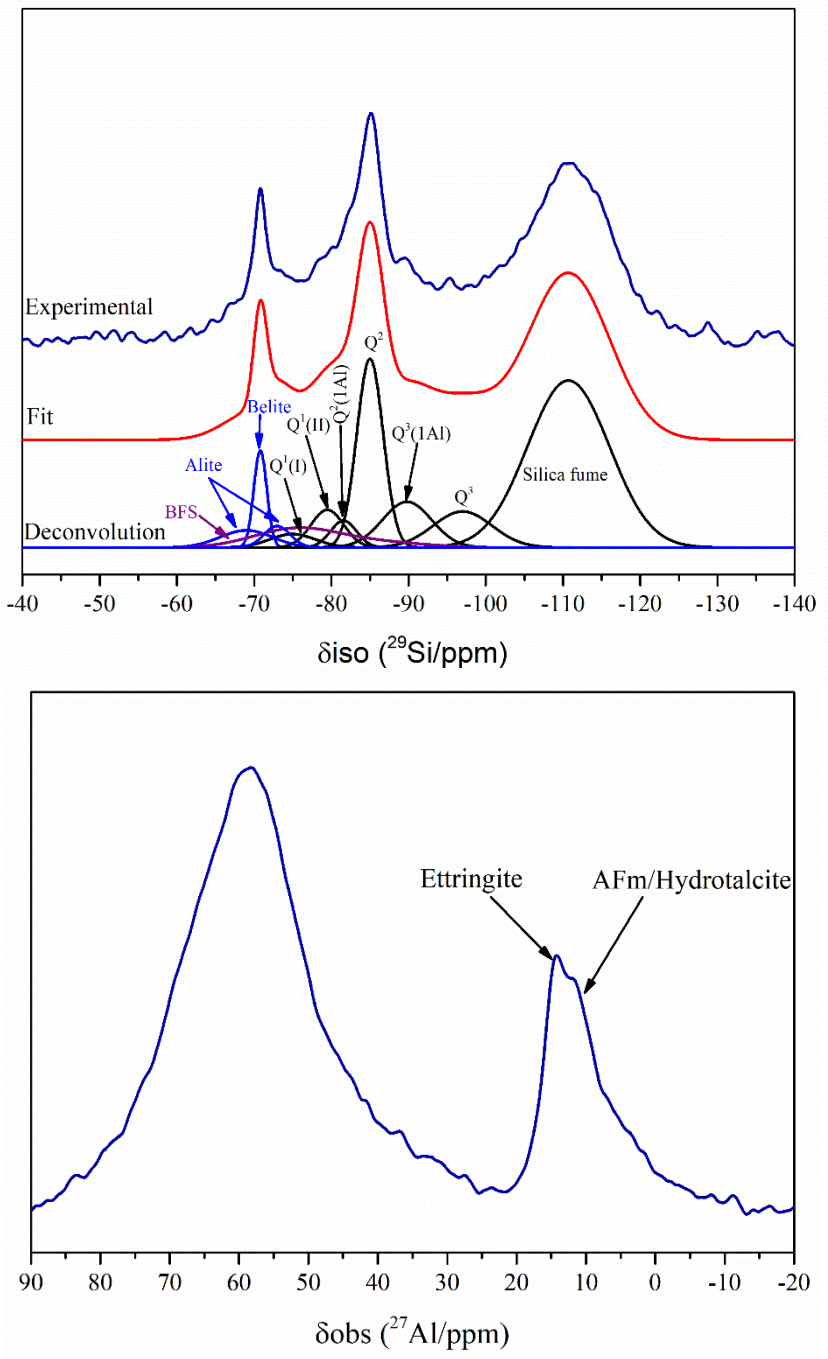

Figure 7. MAS NMR spectra acquired on Cebama reference cement cured for 28 days at 20°C showing: (a) the deconvolution of ^{29}Si MAS NMR spectra; and (b) ^{27}Al MAS NMR spectra.

3.3 Evolution of cement hydration up to, and beyond, 28 days.

Isothermal calorimetry was performed at 20ºC and 40°C for 72 hours (Fig. 8). Due to the sensitivity of the equipment, it was not possible to keep the cement paste at exactly 40°C between the time of the mixture and the actual measurement, therefore, the first 30 minutes of the 40°C data set are not shown. For both temperatures, the same stages of cement hydration could be identified: (1) dissolution of clinker phases and aluminate reaction in tricalcium aluminate; (2) induction period; (3) reaction of alite and formation of C-S-H; and (4) sulfate depletion. When comparing the cumulative heat at these temperatures, it was possible to observe an increase from 90 J/g at 20°C to 120 J/g at 40°C (Figure 8). The reaction rate also increased at the higher temperature, for example, the stage labelled "3" finished after 10 hours at 20°C, but 5 hours at 40°C.

The induction period (labelled 2, Figure 8) at 20°C was longer than observed for non-blended PC cements; this is due to the high replacement of PC with SCMs (Klemczak et al., 2016; Korpa et al., 2008; Lothenbach et al., 2011). BFS is a latent hydraulic material that starts reacting at later ages, and silica fume retards hydration as its reactivity increases only after the pore solution pH is above 10.7 (Langan et al., 2002; Lothenbach et al., 2011; Snellings et al., 2012). The addition of superplasticiser can be also a contributor to this retardation of the acceleration stage (labelled 3) (Siler at al., 2012). The increase in induction period, and the overall lower heat output, when compared with PC (e.g. Jansen et al., 2012) is beneficial for use in the construction of nuclear waste disposal facilities, since prevention of thermal excursion events is desirable (Glasser, 2013). Another interesting observation is the continuous slow release of heat after the sulfate depletion period (labelled 4), which evidences the continuous hydration of the Cebama reference cement paste, especially relating to the reaction of BFS and silica fume at later ages.

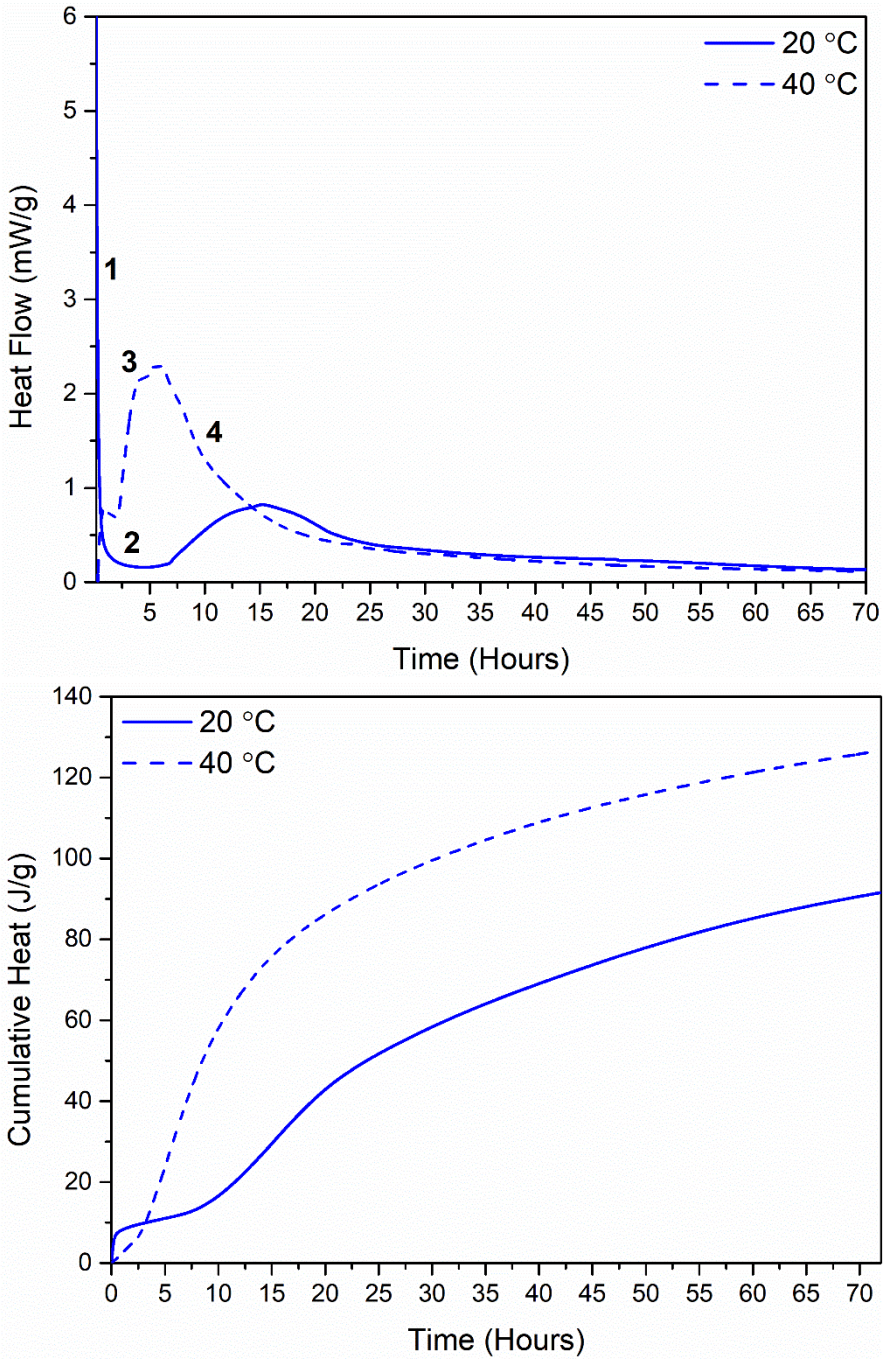

Figure 8. Isothermal calorimetry data for Cebama reference cement paste cured at 20 °C and 40 °C, showing (a) the heat flow; and (b) the cumulative heat.

The SR-XRD patterns acquired at Diamond Light Source over the course of the 18-month investigation are shown in Figure 9. With the high resolution afforded by this synchrotron data set, it was possible to observe, 90 minutes after mixing (Fig. 9a), all of the clinker phases present in the PC (alite, PDF 01-070-1846; belite, PDF 01-086-0398; tricalcium aluminate, PDF 01-070-0839; ferrite, 01-071-0667; and gypsum, PDF 33-0311) in addition to a region of diffuse

scattering from d-spacing values of 6 Å to 3 Å, corresponding to a combination of BFS, silica fume and poorly crystalline C-(A)-S-H. The intensities of the peaks and diffuse scattering changed over time: the clinker phases decreased, with gypsum being completely consumed by ~30 d, while the hydrate phases increased.

After only 90 minutes of curing, hydration of cement resulted in the formation of portlandite (PDF 01-072-0156) and ettringite (PDF 00-041-1451) (Figure 10). This demonstrates the initial rapid reaction of tricalcium aluminate to form ettringite, and also of alite to form portlandite and C-S-H, according to Equations 4 and 5, respectively. The early presence of these hydrate phases, especially portlandite, was previously observed for similar low-pH cement formulations (Jansen et al., 2012; Cau Dit Coumes et al., 2006; Korpa et al., 2008). Indeed, Lothenbach et al. (2014) studied the hydration of low-pH cement blends containing PC and silica fume, from 1 hour up to 7 days, and portlandite was detected in the XRD data.

$$Ca_3Al_2O_6 + 3\,CaSO_4\,2H_2O + 26\,H_2O \rightarrow Ca_6Al_2(OH)_{12}\,3(SO_4)\,26H_2O \quad \text{(Eqn. 4)}$$

$$Ca_3SiO_5 + (1.3 + x)H_2O \rightarrow CaO_{1.7} \cdot SiO_2 \cdot xH_2O + 1.3\,Ca(OH)_2 \quad \text{(Eqn. 5)}$$

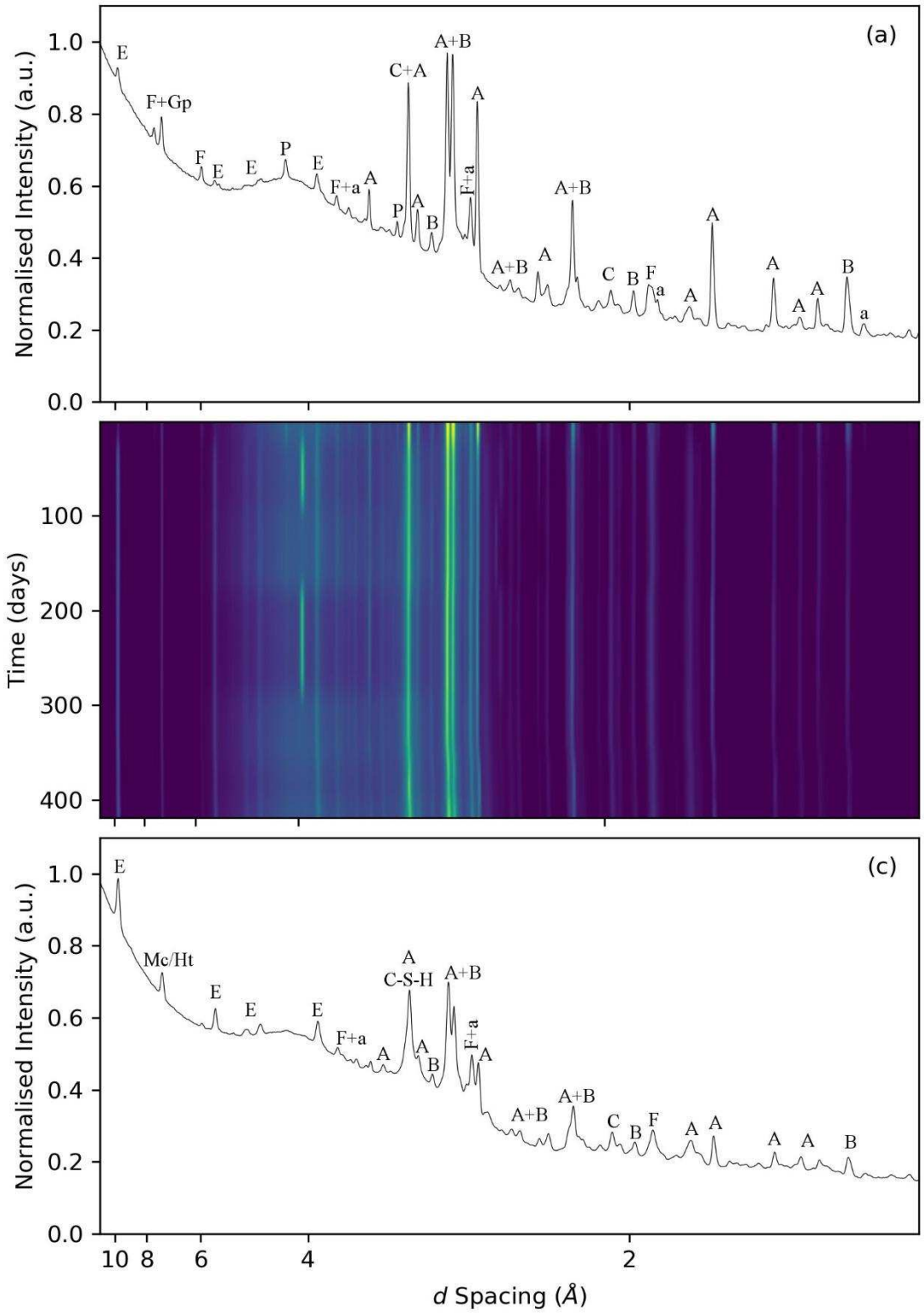

Figure 9. (a) X-ray diffraction pattern for Cebama reference cement at 90 min after mixing; (b) Cebama reference cement peak intensity variation as a function of curing time; (c) X-ray diffraction pattern for Cebama at 1.5 years. Phases are labelled as: A – alite; B – belite; a – aluminate; F – ferrite; Gp – gypsum; P – portlandite; E – ettringite; Mc – monocarboaluminate; Ht – hydrotalcite; C-S-H.

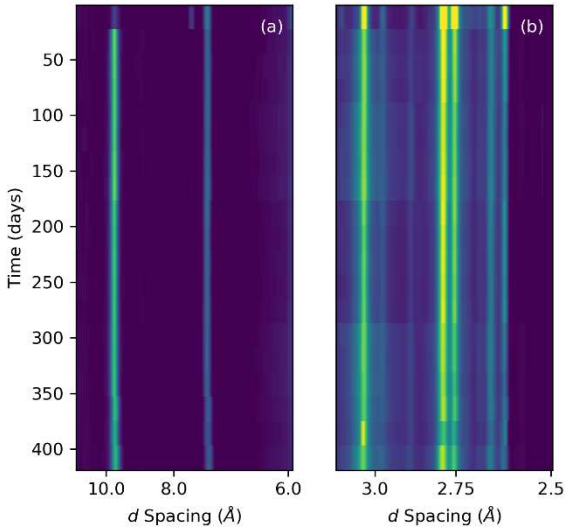

Figure 10. SR-XRD data showing (a) an increase in the intensity of ettringite (at a d-spacing of 9.5 Å) and AFm phases (at a d-spacing of 7.3 Å); and (b) a corresponding decrease in the intensity of the peaks corresponding to alite (d-spacing of 2.97 and 2.77 Å) and belite (at a d-spacing of around 2.88 and 2.75 Å).

With ongoing hydration, as the clinker phases were dissolved and the pH of the cement pore water increased, the pozzolanic reaction of silica fume and BFS also increased (Duchenese et al., 2001; Lothenbach et al., 2011; Snellings et al., 2012). This is evident in Figures 9c and 10b, where a decrease in the intensity of the clinker phases at 18 months can be observed, in addition to a slight decrease in the intensity of the diffuse scattering corresponding to the hydration of BFS and silica fume. Concurrent formation of hydrate phases was observed, including the hydrotalcite-like phase, meixnerite ($Mg_4Al_2(OH)_{14}{\cdot}3H_2O$; PDF 00-014-0191), monocarboaluminate (PDF 01-087-0493) and C-S-H (PDF 19-0052) (Figs. 9c and 10a). The formation of meixnerite arises from the reaction of BFS, which contains MgO, and can have varying Mg/Al ratio depending on the degree of hydration of the BFS and availability of Al (Ke et al., 2016; Richardson, 2013). This will result in a slight variability on the position of the peak, with the incorporation of more Al responsible for a shift to lower angles (Ke et al., 2016).

The presence of monocarboaluminate results from the reaction of tricalcium aluminate with calcite available in the cement clinker, according to Eqn. 6:

$$Ca_3Al_2O_6 + 0.5CaCO_3 + 11.5\,H_2O \rightarrow Ca_4Al_2(OH)_{12}(CO_3)_{0.5} \cdot 5.5\,H_2O \qquad \text{(Eqn. 6)}$$

An increase of the intensity of the peak corresponding to ettringite was also observed with curing time, with the further hydration of tricalcium aluminate. The portlandite peak, at a d-spacing of

~4.7 Å, that was identified at early ages, was no longer present after 18 months of curing, indicating the increased reaction extent of the silica fume and BFS as a function of curing time (Calvo et al., 2010; Dauzeres et al., 2014; Juenger and Siddique, 2015; Lothenbach et al., 2014).

To support quantification of changes in Si-containing phases and C-A-S-H composition as a function of curing time over 18 months, ^{29}Si MAS NMR spectra were recorded on SR-XRD duplicate cement samples at 1, 3, 7, 28 days, and 6, 12 and 18 months, as shown in Figure 11.

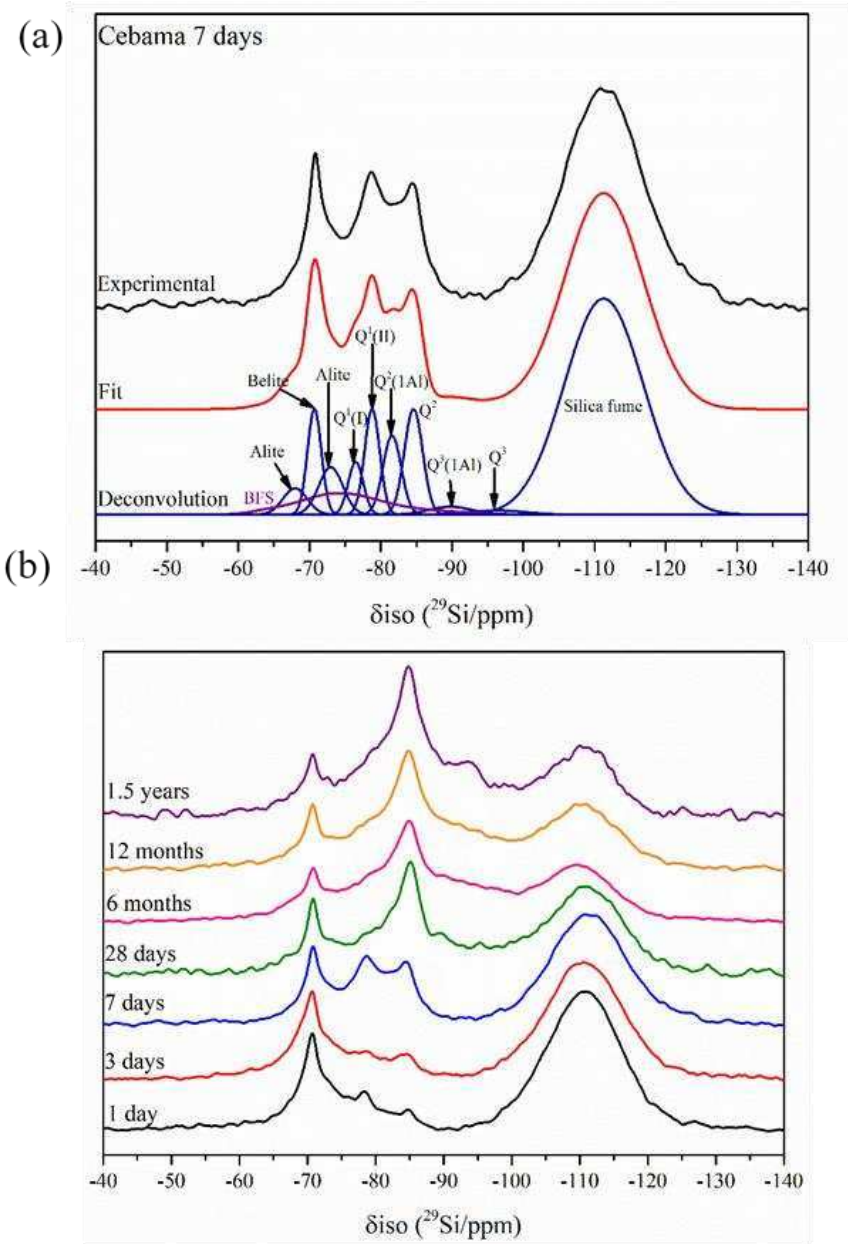

Figure 11. ^{29}Si MAS NMR spectra of Cebama reference cement showing (a) the deconvolution performed at 7 days of curing at 40°C; and (b) spectra recorded a 1, 3, 7 and 28 days, and 6 and 12 months of curing at 40°C. Samples were cured for 18 months at 20°C.

Quantification of the deconvoluted ^{29}Si MAS NMR sites was performed through the integration of the area underneath each Gaussian peak, normalised to the total intensity of the sites, to sum to 100%. These results are shown in Figure 12 and Table 3. The reaction of alite and belite did not occur until after 3 days, when there was a consequent gradual increase in the quantity of C-S-H. In agreement with the SR-XRD data, after approximately 18 months of curing, the presence of alite and belite was still evident. A possible explanation for the observed slow reaction of the clinker phases is the low amount of water used in this formulation (w/s ratio of 0.25), which may affect the final extent of reaction of the different anhydrous phases. Nevertheless, the presence of clinker phases at later curing times has been previously observed in similar blended cements (Lothenbach et al., 2012, 2014).

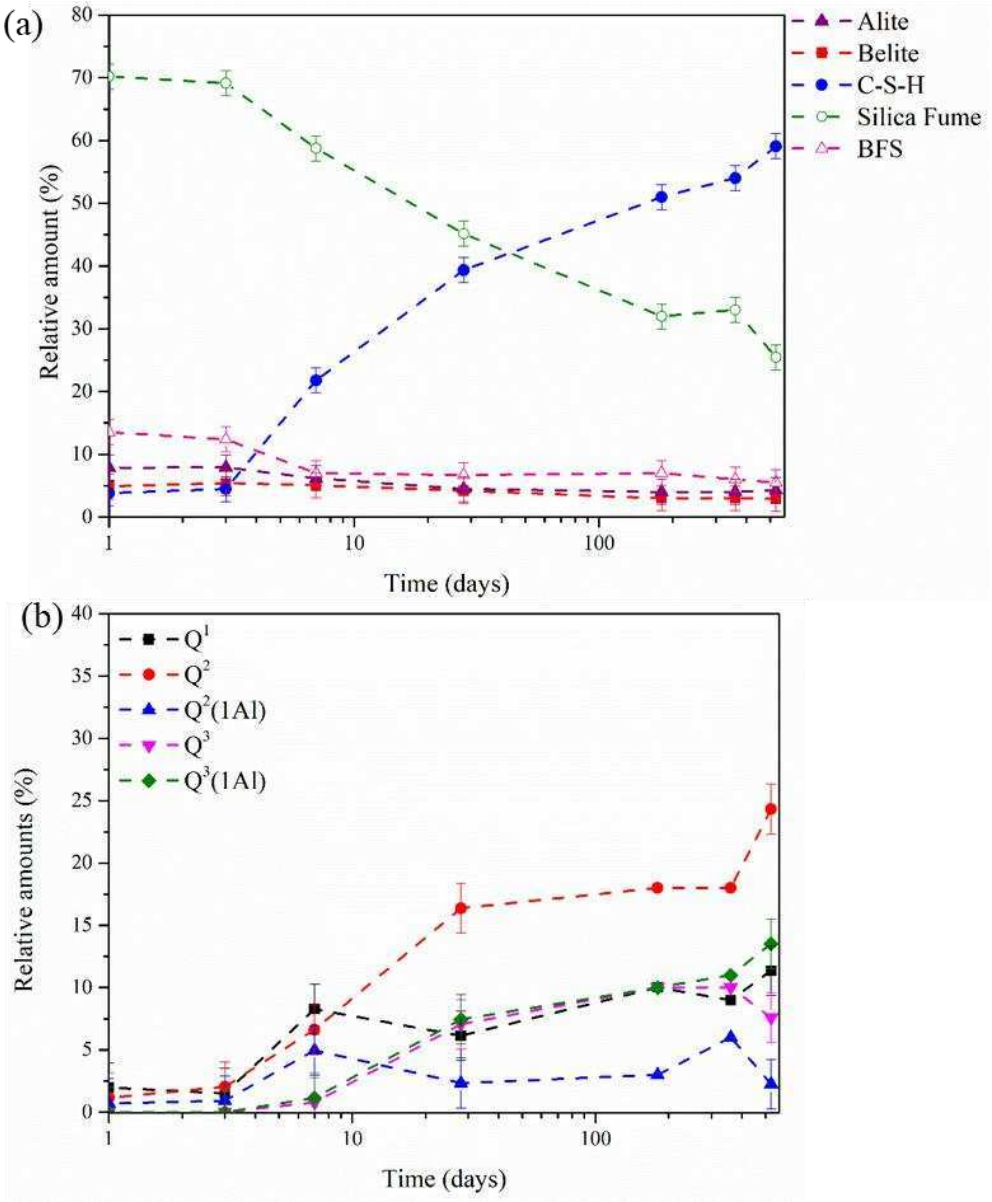

Figure 12. Deconvolution results of the ^{29}Si MAS NMR spectra acquired from the Cebama reference cement paste, based on data shown in Figure 11b, normalised to the total intensity of the reaction product: (a) compares the relative amount of alite, belite, silica fume, BFS and C-A-S-H with curing time, and (b) shows the evolution of the Q^x sites with curing time.

Table 3. Results of deconvolution of ^{29}Si MAS NMR spectra of Cebama reference cement paste as a function of curing time, based on data shown in Figure 11b. The estimated uncertainty in absolute site percentages is ± 2%.

Time	Belite	Alite	Q^1	$Q^2(1Al)$	Q^2	$Q^3(1Al)$	Q^3	Silica fume	BFS
1 day	5%	8%	2%	1%	1%	0	0	70%	14%
3 days	5%	8%	2%	1%	2%	0	0	69%	12%
7 days	5%	6%	8%	5%	7%	1%	1%	59%	7%
28 days	4%	4 %	6%	2%	16%	7%	7%	45%	6%
6 months[a]	3 %	4 %	10 %	3 %	18 %	10 %	10 %	32 %	7 %
12 months[a]	3 %	4 %	9 %	6 %	18 %	11 %	10 %	33 %	6 %
18 months	3%	4%	11%	2%	24%	7%	13%	25%	5%

[a] Sample was cured at 40°C.

There was a small decrease in the relative concentration of Q^1 species in the first 3 days of curing and a concurrent increase in the quantity of the Q^2 sites. After this time, an increase in the relative concentration of both Q^1 and Q^2 sites was observed, as the reaction of the precursor materials increased (Fig. 12b). The appearance of $Q^3(1Al)$ and Q^3 at 7 days evidences the occurrence of some cross-linking of the C-A-S-H, and the consequent increase of the mean chain length (MCL) from 4 ± 2 at 1 day of curing, to 10 ± 3 after 1.5 years of curing (Tables 3 and 4). The incorporation of Al into the C-S-H structure was verified with the increase of the relative concentration of $Q^2(1Al)$ and $Q^3(1Al)$. However, after 28 days, a decrease in the Al/Si ratio was observed (Table 4). This was related to a decrease in the relative amount of $Q^2(1Al)$ after 7 days of curing, and a slight decrease of the relative amount of $Q^3(1Al)$ after 28 days of curing, as shown in Figure 12b. A possible explanation is a greater degree of reaction of silica fume (relative concentration at 28 days was 45 ± 2% and 25 ± 2% at 18 months) than BFS (relative concentration at 28 days of 6 ± 2% and 5 ± 2% at 18 months), which results in an increase of free Si (from silica fume) available to incorporate into the C-S-H structure, and less Al from the BFS (e.g. Lothenbach et al., 2014).

Table 4. Summary of structural evolution of C-(A)-S-H formed in the Cebama reference cement paste as a function of curing time, based on ^{29}Si MAS NMR deconvolution.

Time	Ca/Si Ratio	Al/Si Ratio	Mean Chain Length (MCL)
1 day	1.2 ± 0.5	0.09 ± 0.02	4 ± 2
3 days	1.0 ± 0.5	0.10 ± 0.02	7 ± 3
7 days	1.1 ± 0.3	0.11 ± 0.02	6 ± 4
28 days	0.9 ± 0.1	0.03 ± 0.02	13 ± 3
6 months	0.9 ± 0.2	0.02 ± 0.02	11 ± 2
12 months	0.9 ± 0.1	0.02 ± 0.02	12 ± 2

18 months	0.9 ± 0.1	0.02 ± 0.02	10 ± 3

The slow reaction of silica fume is apparent in the ^{29}Si MAS NMR deconvolution (Table 3). Until 3 days of curing, almost no reaction with silica fume occurred, however, after 7 days, a gradual increase in the reaction of silica fume occurred, with the relative concentration of this material decreasing from 70 ± 2% at 1 day to 25 ± 2% after 18 months. The presence of silica fume, even after 18 months of curing, is likely due to the high percentage used in this cement system (around 39%). Indeed, in a similar formulation where 40% of silica fume was used, the presence of this material was still visible at 3.5 years (Lothenbach et al., 2014). Having high amounts of silica fume increases the likelihood of agglomeration, decreasing the reactivity by reducing its characteristic high surface area for reaction (Lothenbach et al., 2011, 2014; Monzo et al., 2011).

Blast furnace slag was also observed to react slowly (Fig. 12a, Table 3), as has previously been documented for this material; BFS has been shown to be present in cement even after 20 years of curing (Taylor et al., 2010). It has been suggested that the early hydration of BFS is due to reaction with alkali hydroxide, and subsequently reaction with portlandite (Roy et al., 1983; Pal et al., 2003). Therefore, it should be expected that where there is reduced availability of portlandite, as observed for the Cebama reference cement in the current study, there should also be a decrease in the reactivity of BFS. Moreover, the lower w/s ratio used in the formulation will have an impact also in the BFS reactivity, as it is a hydraulic material.

From the deconvolution of the ^{29}Si MAS NMR spectra, it was possible to observe a decrease in the Ca/Si ratio as a function of time, although this seems to be within the error (Table 4). This is expected since the reaction of mainly silica fume, but also of BFS, leads to a decrease of the Ca/Si ratio (Juenger et al., 2015; Lothenbach et al., 2011; Richardson, 2000). The characteristic Ca/Si ratio of low-pH cements can very between 1.2 and 0.8, and should be lower than 1.1 to provide a low-pH pore solution (Calvo et al., 2010; Stronach and Glasser, 1997). This was achieved after only 28 days of curing.

Finally, the porosity of the Cebama reference cement paste was assessed at later curing times than 28 days, by XCT (macroporosity) and MIP (microporosity, Figure 6). For samples cured at 40°C for 6 and 12 months, the pore entry size diameter, ascertained by MIP, allocated the bulk of the pores to pore entry sizes below 0.15 µm. The total porosity obtained by this technique was ~ 9 ± 2%, a decrease from ~19% at 28 days, caused by the presence of a greater amount of cement hydrate phases at later curing times. The macroporosity appeared to increase from ~3% at 28 days curing to 4.5 ± 0.9% and 2.8 ± 0.9% at 6 and 12 months, respectively. However,

these values are within the uncertainty of the measurement, indicating that the porosity did not alter greatly over a 12-month duration.

3.4 *Application of findings to geological disposal of nuclear waste.*

Since the long-term evolution of low-pH cements is generally less well-understood than PC, the detailed characterisation of the long-term changes in phase assemblage determined in the current study provides a useful baseline for future experimental and modelling studies of geological disposal facility cement materials. The main functional requirement of low-pH cements to be utilised in nuclear waste disposal is that the pore fluid should have a pH of < pH 11. Pore solutions with a pH above this value have the potential to degrade bentonite clay buffer, thus reducing the integrity of the disposal system. In the present study, information regarding the composition and quantity of C-(A)-S-H as a function of curing time, shows that this pore solution pH value has likely been achieved, exemplified by the Ca/Si ratio being less than 1.1 after only 28 days of curing. To confirm this, thermodynamic modelling of the cement, using the data presented in the current study as a baseline, is currently being performed by Cebama project partners.

The data presented in the current investigation provide a valuable baseline for experimental and modelling studies of groundwater – low-pH cement interactions, allowing phase stability, thermodynamic values and rate constants to be determined. This may be especially important given the slow hydration kinetics of the Cebama reference cement paste; if durability experiments were to be initiated before the clinker phases have been fully reacted, it is important to understand how groundwater may influence the hydration reaction. Concurrent thermodynamic modelling investigations performed by project partners in the EU Cebama consortium, utilising these data, have recently highlighted the importance of internal relative humidity on the hydration kinetics of the Cebama reference cement paste (Idiart et al., 2019).

Other functional requirements of low-pH cement for geological disposal of nuclear waste include low heat of hydration and low porosity. The data presented here indicate that the porosity of the Cebama reference cement is low, and does not alter significantly over a 12-month period, suggesting that there may be negligible groundwater diffusion through the cement prior to repository closure. The heat of hydration was also found to be lower than for PC, and the influence of curing at 40°C, which is considered by waste management authorities to be the realistic temperature for a geological disposal facility (*pers. comm*), was determined to not significantly influence the hydration reaction.

4. Conclusions

The changes in mineralogy, microstructure (porosity) and nanostructure, over an 18-month period, of a low-pH reference cement developed for use in research and development associated with nuclear waste geological disposal facility construction, were determined. The Cebama reference cement, with high percentages of replacement of Portland cement by silica fume and BFS, was shown to react slowly. Analysis by SR-XRD and ^{29}Si MAS NMR, showed the presence of unreacted Portland cement, BFS and silica fume at 28 days of curing, at both 20°C and 40°C. The main hydrate phases were C-A-S-H, ettringite, AFm phases and hydrotalcite-like phases, such as meixnerite. In respect to the different curing temperatures used, no significant differences were observed in the final phase assemblage and porosity (after 28 days), only a slight increase of the hydration reaction was apparent. Due to the high replacement percentage of PC by silica fume and BFS, and the low w/s ratio, clinker phases, silica fume and BFS were still present after 18 months of curing. Despite this, slow reaction of silica fume and BFS occurred, resulting in the formation of C-A-S-H, with a Ca/Si ratio that decreased with time. This lower Ca/Si ratio (of < 1.1) is a requirement for this type of low-pH cement to be utilised in a geological disposal facility, since is lowers the pore solution pH. The data presented herein provide a benchmark for ongoing and future studies of low-pH cements in geological disposal environments, over long time scales.

Acknowlegdements

The authors wish to acknowledge funding for this research from Radioactive Waste Management and the European Commission Horizon 2020 Research and Training Programme, Cebama, of the European Atomic Energy Community (EURATOM), under grant agreement number 662147. We are grateful to Cebama WP1 consortium members for useful discussions, and particularly to Tapio Vehmas for provision of cement materials, and Alba Valls for her endless patience in the management of the project partners. CLC wishes to acknowledge EPSRC for the award of an Early Career Research Fellowship (EP/N017374/1) and HP wishes to acknowledge EPSRC for funding awarded under grant agreement EP/R01924X/1 (CHIMP). The participation of BW was supported by the EPSRC through grant EP/P013171/1. We wish to thank and acknowledge Dr Sandra van Meurs, The University of Sheffield, for her assistance in collection of MAS NMR data, Dr Oday Hussein, The University of Sheffield, for assistance with MIP data collection, Professor

John L. Provis for insightful discussions about cement hydration and Amy Shelton (RWM) for stakeholder input. We acknowledge Diamond Light Source for time on Beamline I11 LDE under Proposal EE10038 and Dr. Claire Murray for assistance with experiments. This research was performed, in part, at the MIDAS Facility, at the University of Sheffield, which was established with support from the Department of Energy and Climate Change.

References

Andersen, M. D., Jakobsen, H. J., Skibsted J., 2003. Incorporation of aluminum in the calcium silicate hydrate (C−S−H) of hydrated Portland cements: A high-field ^{27}Al and ^{29}Si MAS NMR investigation, 42, 2280 – 2287. https://doi.org/10.1021/ic020607b.

Bach, T., Cau-Dit-Coumes, C., Pochard, I., Nonat, A. , 2011. Retention of alkalis by hydrated low-pH cements designed for underground radioactive waste repositories, in: 13th Int. Congr. Chem. Cem., 1 – 7.

Bernal, S. A., Provis, J. L., Walkley, B., San, R., Gehman, J. D., Brice, D. G., Kilcullen, A. R., Duxson, P., Van Deventer, J. S. J., 2013. Gel nanostructure in alkali-activated binders based on slag and fly ash , and effects of accelerated carbonation. Cem. Concr. Res. 53, 127 – 144. doi:10.1016/j.cemconres.2013.06.007.

Calvo, J. L. G., Hidalgo, A., Alonso, C., Luco, L. F., 2010. Development of low-pH cementitious materials for HLRW repositories Resistance against ground waters aggression. Cem. Concr. Res. 40, 1290 - 1297. doi:10.1016/j.cemconres.2009.11.008.

Cau Dit Coumes, C., Courtois, S., Nectoux, D., Leclercq, S., Bourbon, X., 2006. Formulating a low-alkalinity, high-resistance and low-heat concrete for radioactive waste repositories. Cem. Concr. Res. 36, 2152 – 2163. doi:10.1016/j.cemconres.2006.10.005.

Codina, M., Cau-dit-Coumes, C. , Le Bescop, P., Verdier, J., Ollivier, J. P., 2008. Design and characterization of low-heat and low-alkalinity cements. Cem. Concr. Res. 38, 437 - 448. doi:10.1016/j.cemconres.2007.12.002.

Dauzères, A., Le Bescop, P., Cau-Dit-Coumes, C., Brunet, F., Bourbon, X., Timonen, J., Voutilainen, M., Chomat, L., Sardini, P., 2014. On the physico-chemical evolution of low-pH and CEM I cement pastes interacting with Callovo-Oxfordian pore water under its *in situ* CO_2 partial pressure. Cem. Concr. Res. 58, 76–88. doi:10.1016/j.cemconres.2014.01.010.

Duchesne, J., Bérubé, M. A., 2001. Long-term effectiveness of supplementary cementing materials against alkali-silica reaction, Cem. Concr. Res. 31, 1057–1063. doi:10.1016/S0008-8846(01)00538-5.

Glasser, F. P., 2013. Cements in Radioactive Waste Disposal (IAEA-TECDOC-CD-1701). International Atomic Energy Agency (IAEA).

Holt, E., Leivo, M., Vehmas T., 2014. Low-pH concrete developed for tunnel end plugs used in nuclear waste containment. In: Concrete Innovation Conference 2014 (CIC2014), 1 – 8.

Idiart, A., Laviña, M., Olmeda, J., 2019. Influence of internal relative humidity on the hydration of a low-pH cement. A modelling study. Proc. Third Annu. Work. Horiz. 2020 Cebama Proj., 101–111.

Jansen, D., Goetz-Neunhoeffer, F., Lothenbach, B., Neubauer, J., 2012. The early hydration of

Ordinary Portland Cement (OPC): An approach comparing measured heat flow with calculated heat flow from QXRD. Cem. Concr. Res. 42, 134 – 138. doi:10.1016/j.cemconres.2011.09.001.

Juenger, M. C. G., Siddique R., 2015. Recent advances in understanding the role of supplementary cementitious materials in concrete. Cem. Concr. Res. 78, 71 – 80. doi:10.1016/j.cemconres.2015.03.018.

Ke, X., Bernal, S. A., Provis, J. L., 2016. Controlling the reaction kinetics of sodium carbonate-activated slag cements using calcined layered double hydroxides. Cem. Concr. Res. 81, 24 – 37. doi:10.1016/j.cemconres.2015.11.012.

Klemczak, B., Batog, M., 2016. Heat of hydration of low-clinker cements: Part I. Semi-adiabatic and isothermal tests at different temperature. J. Therm. Anal. Calorim. 123, 1351–1360. doi:10.1007/s10973-015-4782-y.

Korpa, A., Kowald, T., Trettin, R., 2008. Hydration behaviour, structure and morphology of hydration phases in advanced cement-based systems containing micro and nanoscale pozzolanic additives. Cem. Concr. Res. 38, 955 – 962. doi:10.1016/j.cemconres.2008.02.010.

Langan, B. W., Weng, K., Ward, M. A., 2002. Effect of silica fume and fly ash on heat of hydration of Portland cement, Cem. Concr. Res. 32, 1045 – 1051. doi:10.1016/S0008-8846(02)00742-1.

Lothenbach, B., Scrivener, K., Hooton, R. D., 2011. Supplementary cementitious materials. Cem. Concr. Res. 41, 1244 –1256. doi:10.1016/j.cemconres.2010.12.001.

Lothenbach, B., Le Saout, G., Ben Haha, M., Figi, R., Wieland, E., 2012. Hydration of a low-alkali CEM III/B-SiO 2 cement (LAC). Cem. Concr. Res. 42, 410 – 423. doi:10.1016/j.cemconres.2011.11.008.

Lothenbach, B., Rentsch, D., Wieland, E., 2014. Hydration of a silica fume blended low-alkali shotcrete cement. Phys. Chem. Earth. 70 – 71, 3 – 16. doi:10.1016/j.pce.2013.09.007.

Massiot, D., Fayon, F., Capron, M., King, I., Le Calvé, S., Alonso, B., Durand, J. O., Bujoli, B., Gan, Z., Hoatson, G., 2002. Modelling one- and two-dimensional solid-state NMR spectra, Magn. Reson. Chem. 40, 70 – 76. doi:10.1002/mrc.984.

Monzó, J., Martínez-Velandia, D., Payá, J., Borrachero, M. V., 2011. Effect of sonication on the reactivity of silica fume in Portland cement mortars. Adv. Cem. Res. 23, 23–31. doi:10.1680/adcr.8.00027.

Murray, C. A., Potter, J., Day, S. J., Baker, A. R., Thompson S. P., Kelly, J., Morris, C. G., Yang, S., Tang, C. C., 2017. New synchrotron powder diffraction facility for long-duration experiments. J. Appl. Cryst. 50, 172 – 183. doi: 10.1107/S1600576716019750.

Myers, R. J., Bernal, S. A., Provis, J. L., 2014. A thermodynamic model for C-(N-)A-S-H gel: CNASH_ss. Derivation and validation. Cem. Concr. Res. 66, 27 - 47. doi:10.1016/j.cemconres.2014.07.005.

Myers, R. J., Bernal, S. A., Gehman, J. D., Van Deventer, J. S. J., Provis, J. L., 2015. The role of Al in cross-linking of alkali-activated slag cements. J. Am. Ceram. Soc. 98, 996 – 1004. doi:10.1111/jace.13360.

Pal, S. C., Mukherjee, A., Pathak, S. R., 2003. Investigation of hydraulic activity of ground granulated blast furnace slag in concrete. Cem. Concr. Res. 33, 1481 – 1486.

doi:10.1016/S0008-8846(03)00062-0.

Prentice, D. P., Bernal, S. A., Bankhead, M., Hayes, M., Provis, J. L., 2018. Phase evolution of slag-rich cementitious grouts for immobilisation of nuclear wastes. Adv. Cem. Res. 30, 345 – 360. https://doi.org/10.1680/jadcr.17.00198.

Richardson, I. G., 2000. Nature of the hydration products in hardened cement pastes. Cem. Concr. Compos. 22, 97–113. doi:10.1016/S0958-9465(99)00036-0.

Richardson, I. G., 2004. Tobermorite/jennite- and tobermorite/calcium hydroxide-based models for the structure of C-S-H: Applicability to hardened pastes of tricalcium silicate, β-dicalcium silicate, Portland cement, and blends of Portland cement with blast-furnace slag, metakaolin, or silica fume. Cem. Concr. Res. 34, 1733 – 1777. doi:10.1016/j.cemconres.2004.05.034.

Richardson, I. G., 2008. The calcium silicate hydrates. Cem. Concr. Res. 38, 137 – 158. doi:10.1016/j.cemconres.2007.11.005.

Richardson, I. G., Black, L., Skibsted, J., Kirkpatrick, R. J., 2010. Characterisation of cement hydrate phases by TEM, NMR and Raman spectroscopy, Adv. Cem. Res. 22, 233 – 248. doi:10.1680/adcr.2010.22.4.233.

Richardson, I. G., 2013. The importance of proper crystal-chemical and geometrical reasoning demonstrated using layered single and double hydroxides. Acta Crystallogr. Sect. B Struct. Sci. 69, 150–162. doi:10.1107/S0108768113003765.

Richardson, I. G., 2014. Model structures for C-(A)-S-H(I), Acta Crystallogr. Sect. B Struct. Sci. Cryst. Eng. Mater. 70, 903–923. doi:10.1107/s2052520614021982.

Richardson, I. G., Li, S., 2018. Composition and structure of an 18-year-old 5M KOH-activated ground granulated blast-furnace slag paste. Constr. Build. Mater. 168, 404 – 411. doi:10.1016/j.conbuildmat.2018.02.034.

Roy, D. M., Idorn, G. M., 1983. Hydration, structure, and properties of Blast Furnace Slag cements, mortars, and concrete, ACI J. Proc. 79, 445 – 457. doi:10.14359/10919.

Scrivener, K., Snellings, R., Lothenbach, B., 2016. A Practical Guide to Microstructural Analysis of Cementitious Materials, CRC Press, Taylor & Francis Group.

Siler, P., Kratky, J., De Beli, N., 2012. Isothermal and solution calorimetry to assess the effect of superplasticizers and mineral admixtures on cement hydration. J. Therm. Anal. Calorim., 107, 313 – 320. doi:10.1007/s10973-011-1479-8.

Snellings, R., Mertens, G., Elsen, J., 2012. Supplementary Cementitious Materials. Rev. Mineral. Geochem. 74, 211 – 278. doi:10.2138/rmg.2012.74.6.

Stronach, S. A., Glasser, F. P., 1997. Modelling of the impact of abundant geochemical components on the phase stability and solubility of the CaO-SiO_2-H_2O system at 25°C: Na^+, K^+, SO_4^{2-}, Cl^- and CO_3^{2-}. Adv. Cem. Res. 9, 167–181. https://doi.org/10.1680/adcr.1997.9.36.167.

Taylor, R., Richardson, I. G., Brydson, R. M. D., 2010. Composition and microstructure of 20-year-old ordinary Portland cement-ground granulated blast-furnace slag blends containing 0 to 100% slag. Cem. Concr. Res. 40, 971 – 983. doi:10.1016/j.cemconres.2010.02.012.

Thompson, S. P., Parker, J. E., Potter, J., Hill, T. P., Birt, A., Cobb, T. M., Yuan, F., Tang, C. C., 2009. Beamline I11 at Diamond: A new instrument for high resolution powder diffraction.

Rev. Sci. Instrum. 80, 075107. doi:10.1063/1.3167217.

Thompson, S. P., Parker, J. E., Marchal, J., Potter, J., Birt, A., Yuan, F., Fearn, R. D., Lennie, A. R., Street, S. R., Tang, C. C., 2011. Fast X-ray powder diffraction on I11 at Diamond, J. Synchrotron Radiat. 18, 637–648. doi:10.1107/s0909049511013641.

Walkley B., Provis J. L., 2019. Solid-state nuclear magnetic resonance spectroscopy of cements. Mater. Today Adv. 1, 100007. https://doi.org/10.1016/j.mtadv.2019.100007.

Vehmas, T., Schnidler, A., Loija, M., Leivo, M., Holt, E., 2016. Reference mix design and castings for low-pH concrete for nuclear waste repositories. Proc. First Annu. Work. Horiz. 2020 Cebama Proj., 101–111. doi:10.5445/KSP/1000068889.

***Declaration of Interest Statement**

Declaration of interests

☒ The authors declare that they have no known competing financial interests or personal relationships that could have appeared to influence the work reported in this paper.

☐The authors declare the following financial interests/personal relationships which may be considered as potential competing interests: